The structure and phase transition of $(CH_3NH_3)_3Sb_{2(1-x)}Bi_{2x}Cl_9$ mixed crystals

1996 J. Phys.: Condens. Matter 8 367

(http://iopscience.iop.org/0953-8984/8/4/004)

J. Phys.: Condens. Matter **8** (1996) 367–381. Printed in the UK

The structure and phase transition of $(CH_3NH_3)_3Sb_{2(1-x)}Bi_{2x}Cl_9$ mixed crystals

R Jakubas†, G Bator†, J Zaleski‡, A Pietraszko§ and R Decressain‖

† Institute of Chemistry, University of Wroclaw, F Joliot–Curie 14, PL-50383 Wroclaw, Poland
‡ Institute of Chemistry, University of Opole, PL-45-951 Opole, Oleska 48, Poland
§ Institute of Low-Temperature and Structure Research of the Polish Academy of Science, Okólna 2, PL-50-422 Wroclaw, Poland
‖ Laboratoire de Dynamique et Structures des Matériaux Moléculaires (UA No 801), UFR de Physique, Université de Lille 1, F-59655 Villeneuve d'Ascq Cédex, France

Received 7 March 1995, in final form 2 October 1995

Abstract. The phase transition and molecular motions of methylammonium cations are studied in the temperature range from 110 to 450 K in the $(CH_3NH_3)_3Sb_{2(1-x)}Bi_{2x}$ ($x = 0.22$, 0.345) (MACAB) crystal by x-ray DSC, dilatometric, dielectric and ^{1}H NMR techniques. It is shown that MACAB ($x = 0.22$) undergoes a structural phase transition at 222 K. The second moment of the ^{1}H NMR line (M_2) and the temperature dependence of spin lattice relaxation time (T_1) results are interpreted in terms of $(CH_3NH_3)^+$ ion dynamics. In the high-temperature phase (I) the cations undergo isotropic reorientations. In the low-temperature phase (II) only one of three cations is still disordered, whereas the two others perform a C_3 type of reorientation about their C–N axes. It is revealed that substitution of Sb by Bi atoms influences the dynamics of the methylammonium cations and the nature of the structural phase transition.

1. Introduction

$(CH_3NH_3)_3Sb_2Cl_9$ (MACA) and $(CH_3NH_3)_3Bi_2Cl_9$ (MACB) belong to a family of alkylammonium compounds of the general formula $[(CH_3)_nNH_{4-n}]_3Me_2X_9$ (Me = Sb, Bi; X = Cl, Br, I, $n = 1, \ldots, 4$). The methylammonium salts ($n = 1$) exhibit structural phase transitions leading to low-temperature ferroelectric, ferroelastic, antiferroelectric and ferrielectric [1] ordered phases. Mechanisms of phase transitions were related to decrease of reorientational motions of methylammonium cations at T_c [1–3]. They were corroborated by the ^{1}H NMR studies (T_1, spin lattice relaxation time, and M_2, second moment of the ^{1}H NMR line) on some methylammonium crystals [4–6].

MACA and MACB appear to be isomorphous at room temperature and crystallize in the orthorhombic system, space group $Pmna$, $Z = 4$. The antimony analogue undergoes a structural first-order phase transition at 208 K [7], whereas the bismuth one reveals a more complex sequence of phase transitions: at 247 K a weak first-order transition and at about 349 K a diffuse second-order type of transition with no change in the symmetry [8, 9].

The phase transition of MACB at 247 K has been detected by NQR [3], DSC and recently also by the dielectric technique [10]. The Raman studies on single crystals of MACA [11] and IR studies on MACB [12] corroborated the progressive ordering of the methylammonium cations on decreasing temperature. A rapid freezing of the motion of cations at T_c in MACA was corroborated by results of NMR, dielectric and dilatometric studies [7, 13].

0953-8984/96/040367+15$19.50

The present studies were carried out to obtain information on the substitution effect of Sb by Bi atoms on the phase transition and molecular dynamics of methylammonium cations in mixed $(CH_3NH_3)_3Sb_{2(1-x)}Bi_{2x}Cl_9$ crystals.

2. Experimental details

The $(CH_3NH_3)_3Sb_{2(1-x)}Bi_{2x}$ crystals were obtained in a reaction of the stoichiometric amounts of $(BiO)_2CO_3$, Sb_2O_3 and $(CH_3NH_3)Cl$ with excess of HCl. Single crystals were grown from an aqueous solution at constant room temperature. The concentration of Bi atoms was estimated assuming that the density of crystals changes linearly with substitution of antimony by bismuth atoms ($x = 0,\ d = 2.11$ g cm^{-3}; $x = 1,\ d = 2.67$ g cm^{-3}).

Linear thermal expansion was measured using a thermomechanical analyser, Perkin–Elmer TMS-2. The single crystals used in the measurements were prepared in the form of thin plates ($5 \times 5 \times 2$ mm^3). The values of anomalies near the phase transition temperature were reproducible to 10% in sample dimension. The accuracy of thermal expansion determination was about 2%.

Differential scanning calorimeter (DSC) measurements were performed using a Perkin–Elmer DSC-7 calorimeter with a heating/cooling rate of 10 K min^{-1}.

For dielectric measurements samples of dimensions $5 \times 5 \times 1$ mm^3 were cut perpendicularly to the corresponding crystal axes of MACAB. The plates were silver painted. The complex electric permittivity, $\varepsilon^* = \varepsilon' - i\varepsilon''$, was measured using an HP 4284A Precision *LCR* meter in the frequency range 100 Hz–1 MHz and an HP 4191A RF impedance analyser in the frequency range 30–900 MHz. The measurements were performed in the temperature range 140–300 K. The temperature was changed at a rate of 0.1 K min^{-1} in the vicinity of T_c and 0.5 K min^{-1} elsewhere in the case of the measurements in the low-frequency region. For the microwave-frequency region the temperature was stabilized and controlled by a UNIPAN temperature controller type 650 with fluctuations less than ± 0.1 K.

The overall error for the real part of the complex electric permittivity, ε', was less than 5%. The overall error for the imaginary part of the complex electric permittivity, ε'', was less than 7%.

The NMR measurements were carried out at 100 MHz on a Bruker CXP 100 spectrometer. The powdered crystals were put in a glass tube and dried *in vacuo* for longer than 10 h and then sealed with nitrogen gas. The spin–lattice relaxation time T_1 was measured with the magnetization recovery pulse sequence $(\pi, -\tau, -\pi/2)_n$. The measurements were carried out between 100 and 400 K with an accuracy of 1 K. The reproducibility of the results was checked by recording the NMR spectra during cooling and heating.

The x-ray Bond diffractometer with low-temperature attachment used in investigations of the temperature dependence of lattice parameters and the thermal expansion indicates a deformation of the crystal lattice with a relative accuracy better than $\Delta a/a = 10^{-5}$. The automatic Bond diffractometer, type KM4-Bond, is a four-circle fully automatic x-ray diffractometer with special x-ray optics (long collimator, monochromator, special slits and software [14]). The high 2θ angles ($2\theta = 166^\circ$) are measured at the two symmetrical positions of the samples with a precision in ω angles of $\pm 0.001^\circ$. The samples used for x-ray Bond measurements were irregular in shape ($0.8 \times 0.6 \times 0.7$ mm^3). The Bragg angles (all $2\theta > 150^\circ$) for 3 3 16, -3 3 16, 12 8 6, 12 8 -6, 15 2 -13, 15 2 13, 18 6 6, 18 6 -6 reflections were measured on heating over a temperature range 165–295 K using Cu Kα_{12} radiation.

Data for structure determination were collected on a KM-4 KUMA diffractometer with Mo Kα radiation ($\lambda = 0.710\,73$ Å; graphite mononochromator). Lattice parameters were

refined from setting angles of 25 reflections in the $17^\circ < 2\theta < 25^\circ$ range. A summary of the measurement parameters is presented in table 1. A total of 3394 reflections with $2^\circ < 2\theta < 50^\circ$ were collected using the ω–θ scan technique (scan speed, 0.03–0.12° s^{-1}; scan width 0.83°). After merging ($R_{int} = 0.038$) of 1870 independent reflections 1332 had $|F_0| > 4\sigma(|F_0|)$ and were used for structure determination. Two control reflections measured after an interval of 50 reflections show that the intensity variation was negligible. Lorentz and polarization with semiempirical absorption corrections (μ_{Mo} K$\alpha = 87.6$ cm^{-1}) were applied ($trans_{min} = 0.01$, $trans_{max} = 0.03$). The SHELXTL PC program [15] was used for all the structure calculations and drawings.

Table 1. Crystal data for $(CH_3NH_3)_3Sb_{1.31}Bi_{0.69}Cl_9$ and the summary of the measurement parameters.

Empirical formula	$(CH_3NH_3)_3Sb_{1.31}Bi_{0.69}Cl_9$
Crystal size (mm)	0.3 0.3 0.4
Crystal system	Orthorhombic
Space group	*Pnma*
Unit cell dimensions (Å)	$a = 19.605(5)$
	$b = 7.855(2)$
	$c = 13.332(3)$
Volume (Å^3)	2053(1)
Z	4
Formula weight	727.6
Density (calc.)	2.35 g cm^{-3}
Density (meas.)	2.32(1) g cm^{-3}
Absorption coefficient (mm^{-1})	8.76
Temperature (K)	298
Index ranges	$-23 < h < 23,\ 0 < k < 9,\ 0 < 1 < 15$
Reflections collected	3394
Observed reflections	1332 ($F_0 > 4.0\sigma(F_0)$)
Refinement method	full-matrix least-squares
Quantity minimized	$\sum w(F_0 - F_c)^2$
Extinction correction	$\chi = 0.000\,31(2)$, where
	$F^* = F[1 + 0.002\chi^* F^2/\sin(2\theta)]^{-1/4}$
Weighting scheme	$w^{-1} = \sigma^2(F)$
Number of parameters refined	111
Final R indices (obs. data)	$R = 3.79\%,\ wR = 3.57\%$
GOOF	1.65
Data-to-parameter ratio	12:1
Largest difference peak (e Å^{-3})	0.95
Largest difference hole (e Å^{-3})	−0.69

3. Results and discussion

3.1. X-ray studies

From systematic absences the non-centrosymmetrical $Pna2_1$ and the centrosymmetrical *Pnma* space group follows. Solution in the $Pna2_1$ group leads to a higher R factor (5.5%) so the *Pnma* group was chosen. Details of the solution are given in table 1. The space group of $(CH_3NH_3)_3Sb_{1.31}Bi_{0.69}Cl_9$ is the same as the space groups of three closely related compounds β-$Cs_3Sb_2Cl_9$, $Cs_3Bi_2Cl_9$ [16] and $(CH_3NH_3)_3Sb_2Cl_9$ [7].

The structure was solved by the Patterson method and subsequent difference Fourier

synthesis. After the location and refinement of all antimony, bismuth and chlorines on difference Fourier synthesis, there were left six electron peaks (larger than 1 e $Å^{-3}$) located on the *ac* plane and corresponding to three crystallographically non-equivalent cations. Based on electron densities of Fourier peaks on difference synthesis, one may classify the three methylammonium cations as having different degrees of disorder. The N(1)–C(1) cation is almost ordered, while the N(3)–C(3) one occupying the largest polyanionic cavity is most disordered. This is in agreement with the situation found in $(CH_3NH_3)_3Sb_2Cl_9$ [7].

The occupancy factors of Bi and Sb atoms were refined and converged at 0.382 and 0.273 for Sb(1) and Sb(2), respectively. This corresponds to a chemical formula of $(CH_3NH_3)_3Sb_{1.31}Bi_{0.69}Cl_9$.

The electron densities corresponding to N and C atoms are almost the same (with the exception of N(1) and C(1) which could be assigned unambiguously) so the assignment of atom types is based on distances of electron peaks to chlorines. Those characterized by closer distances are assumed to be nitrogens (connected to Cl atoms by N–H$\cdots$Cl bonds). The methylammonium cations are characterized by large thermal motions which is reflected in their large temperature factors. The positional parameters of non-hydrogen atoms are presented in table 2.

Table 2. Atomic coordinates ($\times 10^4$) and equivalent isotropic displacement coefficients ($Å^2 \times 10^3$) of non-hydrogen atoms and site occupation factors for antimony and bismuth atoms of $(CH_3NH_3)_3Sb_{1.31}Bi_{0.69}Cl_9$. The equivalent isotropic U is defined as one-third of the trace of the orthogonalized U_{ij} tensor.

	x	*y*	*z*	U	SOF
Bi(1)	−15(10)	2500	2529(6)	42(1)	0.118
Bi(2)	1749(1)	2500	5825(3)	35(1)	0.227
Sb(1)	−9(5)	2500	2290(3)	41(1)	0.382
Sb(2)	1758(3)	2500	5816(6)	83(2)	0.273
Cl(1)	−715(2)	2500	836(3)	93(2)	
Cl(2)	710(2)	213(4)	1650(3)	92(1)	
Cl(3)	−914(2)	−27(4)	3168(3)	108(1)	
Cl(4)	827(3)	2500	4149(4)	127(2)	
Cl(5)	2543(2)	2500	7276(4)	106(2)	
Cl(6)	2406(2)	214(5)	4962(3)	108(1)	
N(1)	592(9)	2500	9045(14)	129(3)	
C(1)	1224(8)	2500	9309(14)	121(3)	
N(2)	2746(11)	2500	2778(15)	184(3)	
C(2)	2227(12)	2500	2292(18)	155(3)	
N(3)	3948(11)	2500	8946(19)	200(3)	
C(3)	4392(11)	2500	9328(20)	170(3)	

The anionic sublattice of $(CH_3NH_3)_3Sb_{1.31}Bi_{0.69}Cl_9$ is composed of one-dimensional polyanionic $(M_2Cl_9^{3-})_n$ chains composed of corner-connected MCl_6^{3-} octahedra, which are elongated along the *b* axis. The methylammonium cations are located in three different cavities formed by the polyanionic sublattice. They are connected to the anionic sublattice by electrostatic interactions as well as weak N–H$\cdots$Cl bonds.

The projection of the crystal structure of MACAB on the *ac* plane is presented in figure 1.

The bond lengths and angles are presented in table 3. The M–Cl distances fall in two ranges of 2.38–2.64 Å for terminal chlorines and 2.72–2.97 Å for bridging ones. They are in good agreement with values found in the closely related compounds [7, 14],

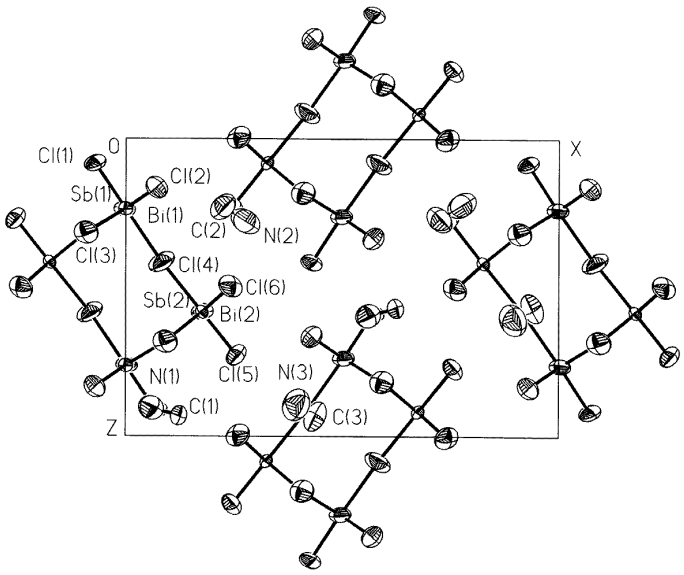

Figure 1. The crystal structure of $(CH_3NH_3)_3Sb_{2(1-x)}Bi_{2x}Cl_9$ ($x = 0.345$) viewed along the b axis.

although the respective ranges are smaller, which indicates that the polyanionic sublattice of $(CH_3NH_3)_3Sb_{1.31}Bi_{0.69}Cl_9$ is less distorted in comparison to other salts.

The obtained N–C distances are very short, which originates from lack of precision in determining true distances because of the large thermal motions of the cations.

It should be noted that Bi atoms tend to substitute Sb(2) atoms more easily (Sb(2):Bi(2) = 0.55:0.45) than Sb(1) atoms (Sb(1):Bi(1) = 0.76:0.24).

The comparison of lattice parameters of caesium and methylammonium chloroantimonates and bismuthates is presented in table 4. The two caesium salts have similar lattice parameters along the a and b axes, while the bismuth salt has a larger c parameter by 0.15 Å. This points out that the substitution of antimony by bismuth atoms does not lead to significant distortion of the crystal lattice.

Comparison of caesium and methylammonium chlorobismuthates reveals that the methylammonium cations are accommodated in the crystal structure by large elongation of the a parameter (realized probably by shifting the polyanionic chains along the a direction), while the b and c parameters rest practically unchanged. This may be understood by assuming that the methylammonium cations are located on the ac plane with long C–N axes of the molecules almost along the a axis.

A different situation takes place in the case of the methylammonium chloroantimonate, where substituting caesium cations by methylammonium, apart from resulting in smaller (than in the bismuth case) elongation along the a axis, also results in a significant elongation of the lattice along the b direction.

Comparison of mixed crystals with the methylammonium salts reveals that substituting antimony atoms by bismuth leads to a diminution of the b parameter as expected. Surprisingly the a parameter is not increased, while the c parameter stays the same. As a result the volume of the unit cell is diminished, leading to a closer-packed structure.

The ratio of Sb to Bi was checked by the EDAX method giving an Sb to Bi ratio of 0.66:0.34, confirming the results obtained by the x-ray diffraction method.

Table 3. Bond lengths (Å) and angles (°) for $(CH_3NH_3)_3Sb_{1.31}Bi_{0.69}Cl_9$.

Sb(1)–Cl(1)	2.382(8)	Cl(1)–Sb(1)–Cl(2)	92.9(2)
Sb(1)–Cl(2)	2.438(7)	Cl(1)–Sb(1)–Cl(3)	88.5(2)
Sb(1)–Cl(3)	2.908(7)	Cl(1)–Sb(1)–Cl(4)	178.0(4)
Sb(1)–Cl(4)	2.972(8)	Cl(2)–Sb(1)–Cl(2″)	94.9(3)
		Cl(2)–Sb(1)–Cl(3)	89.5(1)
Bi(1)–Cl(1)	2.643(13)	Cl(2)–Sb(1)–Cl(3″)	175.3(2)
Bi(1)–Cl(2)	2.573(12)	Cl(2)–Sb(1)–Cl(4)	88.4(3)
Bi(1)–Cl(3)	2.788(13)	Cl(3)–Sb(1)–Cl(3″)	86.1(3)
Bi(1)–Cl(4)	2.718(14)	Cl(3)–Sb(1)–Cl(4)	90.0(1)
		Cl(3″)–Sb(2)–Cl(3′)	84.5(2)
Sb(2)–Cl(3′)	2.889(6)	Cl(4)–Sb(2)–Cl(3′)	90.0(2)
Sb(2)–Cl(4)	2.876(9)	Cl(4)–Sb(2)–Cl(5)	179.0(3)
Sb(2)–Cl(5)	2.482(9)	Cl(4)–Sb(2)–Cl(6)	88.3(2)
Sb(2)–Cl(6)	2.477(6)	Cl(5)–Sb(2)–Cl(3′)	89.3(2)
		Cl(5)–Sb(2)–Cl(6)	92.4(2)
Bi(2)–Cl(3′)	2.873(4)	Cl(6)–Sb(2)–Cl(3′)	91.3(1)
Bi(2)–Cl(4)	2.874(7)	Cl(6)–Sb(2)–Cl(3″)	175.4(2)
Bi(2)–Cl(5)	2.483(6)	Cl(6)–Sb(2)–Cl(6″)	92.9(2)
Bi(2)–Cl(6)	2.492(4)		
		Cl(1)–Bi(1)–Cl(2)	84.1(2)
		Cl(1)–Bi(1)–Cl(3)	86.1(4)
N(1)–C(1)	1.29(2)	Cl(1)–Bi(1)–Cl(4)	173.9(7)
N(2)–C(2)	1.21(3)	Cl(2)–Bi(1)–Cl(2″)	88.5(5)
N(3)–C(3)	1.01(3)	Cl(2)–Bi(1)–Cl(3)	89.5(1)
		Cl(2)–Bi(1)–Cl(3″)	170.1(6)
		Cl(2)–Bi(1)–Cl(4)	91.5(5)
		Cl(3)–Bi(1)–Cl(3″)	90.5(5)
		Cl(3)–Bi(1)–Cl(4)	98.1(2)
Symmetry codes			
		Cl(3″)–Bi(2)–Cl(3′)	85.1(2)
$'\ -X, -Y, 1-Z$		Cl(4)–Bi(2)–Cl(3′)	90.3(1)
$''\ X, 0.5-Y, Z$		Cl(4)–Bi(2)–Cl(5)	180.0(3)
$'''\ -X, 0.5+Y, 1-Z$		Cl(4)–Bi(2)–Cl(6)	88.0(2)
		Cl(5)–Bi(2)–Cl(3′)	89.6(2)
		Cl(5)–Bi(2)–Cl(6)	92.0(1)
		Cl(6)–Bi(2)–Cl(3′)	91.3(1)
		Cl(6)–Bi(2)–Cl(3″)	176.0(1)
		Cl(6)–Bi(2)–Cl(6″)	92.2(2)

Table 4. A comparison of lattice parameters of isomorphous methylammonium and caesium chloroantimonates and bismuthates.

Compound	a (Å)	b (Å)	c (Å)	V (Å^3)	Ref
β-$Cs_3Sb_2Cl_9$	18.663(4)	7.630(20)	13.079(2)	1863	[1]
$Cs_3Bi_2Cl_9$	18.684(4)	7.644(3)	13.227(3)	1889	[1]
$(CH_3NH_3)_3Sb_2Cl_9$	19.660(20)	7.920(5)	13.334(11)	2076	[2]
$(CH_3NH_3)_3Sb_{1.56}Bi_{0.44}Cl_9$	19.640(8)	7.868(3)	13.344(6)	2062	present work
$(CH_3NH_3)_3Sb_{1.31}Bi_{0.69}Cl_9$	19.605(5)	7.855(2)	13.332(3)	2053	present work
$(CH_3NH_3)_3Bi_2Cl_9$	20.422	7.697	13.248	2084	[3]

3.2. Dilatometric studies

The temperature dependence of dilation of MACAB ($x = 0.22$) along the a, b and c axes on heating, measured using a thermomechanical analyser, is shown in figure 2. A

clear, sharp anomaly observed in the vicinity of 223 K with a thermal hysteresis of the order of 2 K indicates a first-order phase transition. Along the b and c axes the crystal expands continuously above T_c with the constant linear coefficient $\bar{\alpha}_c = 2.3 \times 10^{-3}$ K^{-1}, $\bar{\alpha}_c = 1.5 \times 10^{-4}$ K^{-1}, and $\bar{\alpha}_a = -7.7 \times 10^{-4}$ K^{-1}, whereas below 223 K these coefficients increase as the critical point is approached. We should note the relatively large values of the $\bar{\alpha}$ coefficients in the studied temperature range.

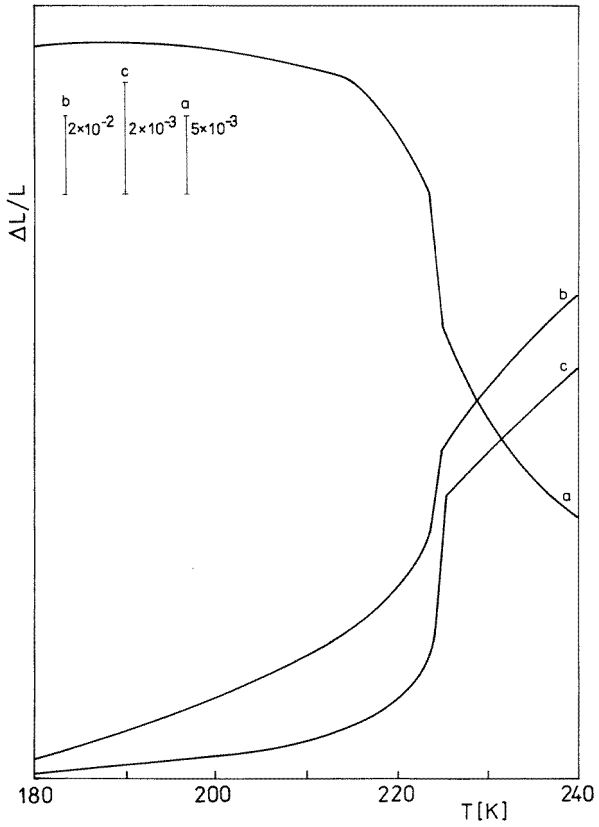

Figure 2. The linear thermal expansion of $(CH_3NH_3)_3Sb_{2(1-x)}Bi_{2x}Cl_9$ ($x = 0.22$) mixed crystals along the a, b and c axes (by thermomechanical analyser).

Table 5. The changes of the linear thermal expansion along the a, b and c axes at T_c, the transition volume and the pressure coefficient dT_c/dp for $(CH_3NH_3)_3Sb_{2(1-x)}Bi_{2x}$ ($x = 0.22$).

Axis	$10^3\,\Delta L/L$	$10^3\,\Delta V/V$	dT_c/dp (10^{-2} K MPa^{-1})
b	+ 16.0		
c	+ 2.40	10.3	17.8
a	− 8.1		

Table 5 shows the size of the anomaly in the thermal dilation of the ($x = 0.22$) samples at the phase transition temperatures along the principal axes. The pressure coefficient of the transition temperature can be estimated by the Clausius–Clapeyron relation:

$dT_c/dp = \Delta V/\Delta S$, where ΔV is the change in molar volume and ΔS the value of the transition entropy.

The dilatometric results for MACAB ($x = 0.22$) are different from those found in crystals of MACA [13]. The pressure coefficient dT_c/dp from measurements on a polycrystalline sample of MACA was estimated to be negative, whereas in the case of MACAB it is positive and rather large in value. In the low-temperature phase of MACAB the thermal dilatation along all directions has a large trail up to the higher temperature, whereas for the MACA crystal a rapid jump in $\Delta L/L$ at T_c is observed (see figure 4 in [13]; the notation of the crystallographic axes was taken as follows: $a = 7.920$, $b = 19.666$ and $c = 13.334$ Å). On the other hand there is good agreement with thermal expansion coefficients above T_c for all directions of both crystals. The present studies show that the replacement of Bi by Sb influence the thermal expansion parameters especially in the phase transition temperature region.

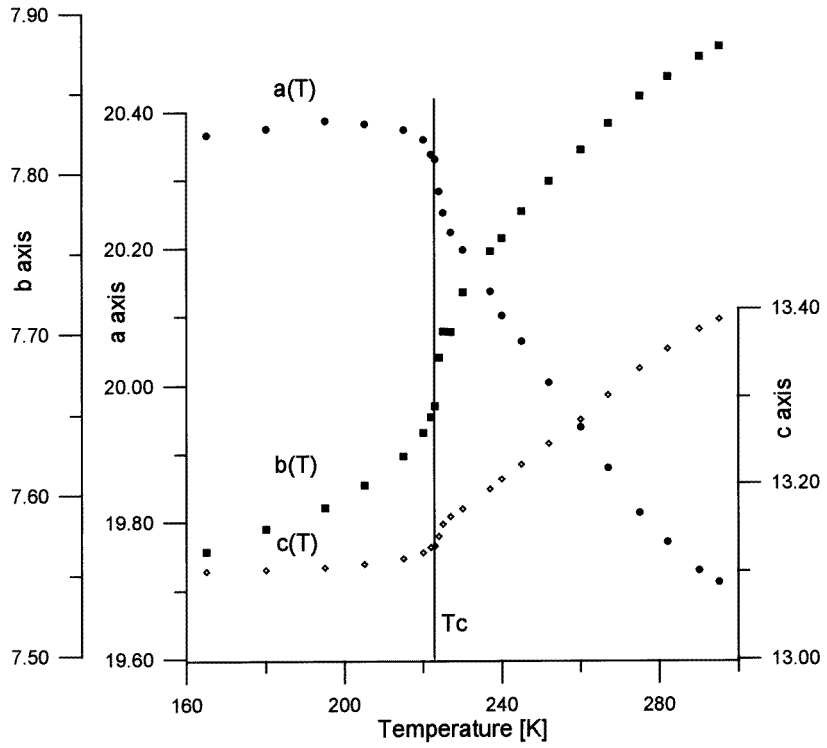

Figure 3. Temperature dependences of the a, b and c lattice parameters of $(CH_3NH_3)_3Sb_{2(1-x)}Bi_{2x}Cl_9$ ($x = 0.345$) in the low-temperature region.

Lattice parameters a, b and c of MACAB ($x = 0.345$) calculated from θ values are plotted as a function of temperature in figure 3. The temperature dependence of the lattice parameters in the phase transition region (near $T_c = 222.5$ K, on heating) indicates that the phase transition is very close to second order (temperature hysteresis lower than 0.5 K), whereas in the case of the $x = 0.22$ crystal the corresponding structural anomaly is clearly of first order. The lack of ordering of the studied reflection profiles indicates that below the transition point the crystal structure probably belongs also to the orthorhombic system.

3.3. DSC

A solid-state phase transition was detected as a pronounced endothermic peak at 223 ± 0.5 K on heating and an exothermic one at 222 ± 0.5 K on cooling (thermal hysteresis, 1.0 K) (see figure 4). The transition enthalpy $\Delta H_{tr} = 5.82$ J g^{-1} determined from the peak area (on heating) and corresponding transition entropy amounts to 18.2 J mol^{-1} K^{-1}. The relatively sharp peak on a DSC curve and the value of the thermal hysteresis indicate that the phase transition is of first rather than of second order.

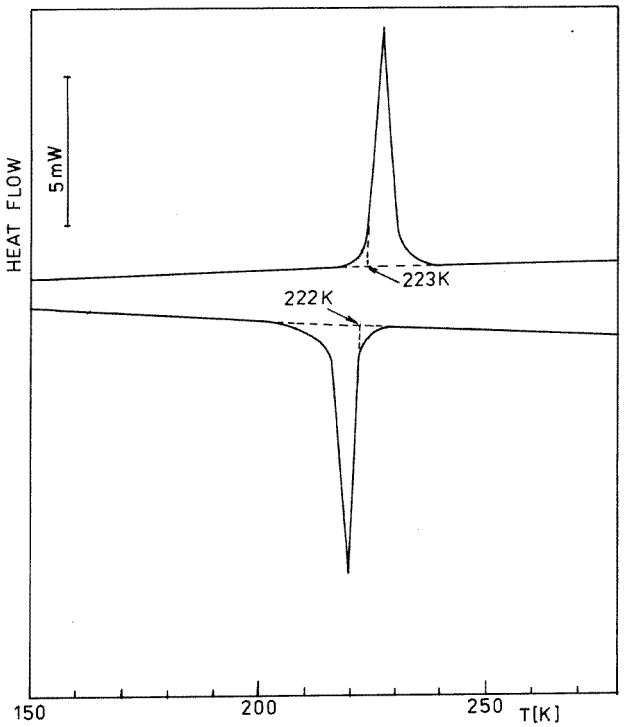

Figure 4. Heat flow curve of $(CH_3NH_3)_3Sb_{2(1-x)}Bi_{2x}Cl_9$ ($x = 0.22$) measured on heating and cooling at 10 K min^{-1}.

The comparison of transition entropy of MACA ($\Delta S \approx 40$ J mol^{-1} K^{-1} [7]) with that of $(CH_3NH_3)_3Sb_{2(1-x)}Bi_{2x}Cl_9$ ($x = 0.22$) shows a diminution of the entropy effect, which points to a distinct decrease in the freedom of rotational motion of the methylammonium cations. For the $(CH_3NH_3)_3Bi_2Cl_9$ crystals the specific heat anomaly resembles that of a phase transition of the second-order type with $\Delta S \approx 4.45$ J mol^{-1} K^{-1} [8]. The DSC studies confirm also that increase of bismuth concentration causes both a distinct decrease of the value of the entropy effect and diminution of the temperature hysteresis.

3.4. NMR

The temperature dependence of the proton second moment M_2 for MACAB ($x = 0.22$) is plotted in figure 5 (M_2 for MACA taken from [7] is added for comparison). The second moment M_2 for MACAB is found not to have any plateau value between 400 and 100 K. Below 400 K with decreasing temperature a continuous increase of M_2 from 1×10^{-8} T^2 up

to 3×10^{-8} T^2 near 220 K is observed. Within phase (II) down to 100 K M_2 continuously increases, faster than in the high-temperature phase, up to 6×10^{-8} T^2. To identify the types of reorientation of $CH_3NH_3^+$ cations contributing to the temperature changes of the proton second moment it is necessary to compare the observed values of M_2 with calculated ones for different possible motional modes. The theoretical M_2 values are reported to be 29, 19, 8 and 0.5×10^{-8} T^2 for the rigid-cation, the C_3 type rotation of the CH_3 group with NH_3 rigid, for both groups reorienting about the C–N bond and for isotropic reorientation, respectively.

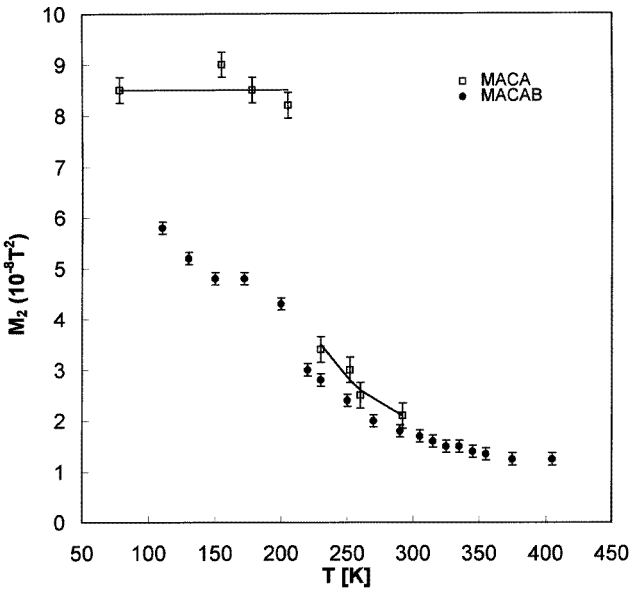

Figure 5. The temperature dependence of the ^{1}H second moment, M_2, for MACAB ($x = 0.22$) ($T_c = 220$ K) and for MACA ($T_c = 208$ K; results after [7]).

The value of the second moment ($\sim 1 \times 10^{-8}$ T^2) at high temperature (400 K) is consistent with a model assuming practically isotropic reorientation of all methylammonium cations. Our x-ray studies at 295 K showed that two of three non-equivalent cations are disordered and the third one (N(1)–C(1)) seems to be more ordered. This means that the increase of the M_2 value between 400 K and 295 K, and down to the phase transition, is undoubtedly connected with the change in the motional state of at least one of the methylammonium cations. In the low-temperature phase the ordering process of the methylammonium cations is still continued. At 100 K $M_2 = 6 \times 10^{-8}$ T^2 is distinctly lower than the value corresponding to the uniaxial rotation of three methylammonium cations ($M_2 = 8 \times 10^{-8}$ T^2). Such a reduction of M_2 is assumed to arise from a fast precessional motion around the C–N bond axis of one of three non-equivalent $CH_3NH_3^+$ cations. From figure 5 it is evident that there are differences in the dynamics of the methylammonium cations for the MACA and MACAB crystals in the vicinity of the phase transition temperature. In MACA at the phase transition there is a rapid freezing of the reorientational motions of methylammonium cations around the C–N axis whereas for MACAB this process is extended over a wide temperature region.

3.5. T_1 measurements

The variation of ^{1}H spin–lattice relaxation time (T_1) with temperature in the range 110–450 K is shown in figure 6. Initially, T_1 increases with decreasing temperature, reaches a maximum at about 400 K and decreases monotonically with further decrease in temperature. In the close vicinity of $T_c = 220$ K a small T_1 anomaly is visible. Below 220 K T_1 decreases monotonically down to 110 K without exhibiting any minimum. Assuming the Arrhenius relation, the activation parameters evaluated from the linear part of the $\log T_1$ vs T^{-1} plot were found to be comparable for the phases I and II and equal to 4.5 kJ mol^{-1}. The low activation energy (E_a) indicates a large freedom of the reorientation of $(CH_3NH_3)^+$ cations in both phases and justifies the absence of a T_1 minimum down to 110 K.

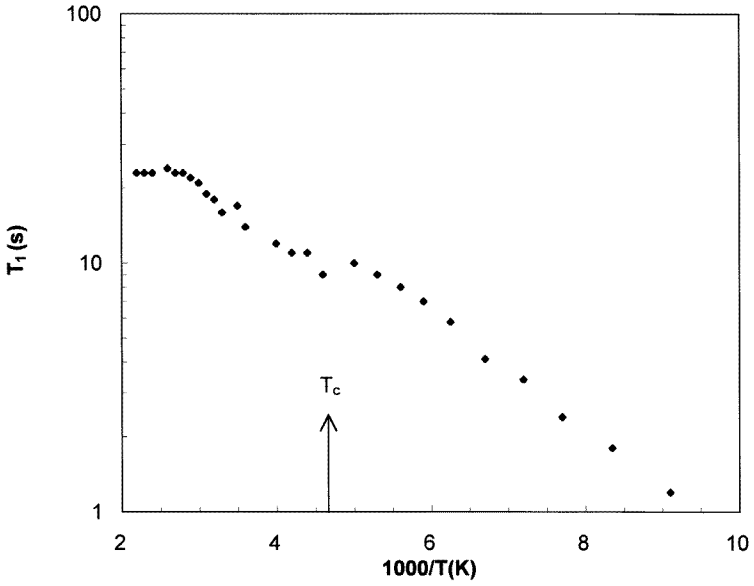

Figure 6. The temperature dependence of the ^{1}H spin–lattice relaxation time for MACAB ($x = 0.22$).

T_1 exhibits a maximum of 25 s at 400 K which may probably be attributed to the spin–rotational interaction. A similar T_1 maximum has been found in other methylammonium compounds $(CH_3NH_3)PbX_3$ [17], $(CH_3NH_3)I$ [18] and $(CH_3NH_3)_2ZnBr_4$ [19], exhibiting self-diffusion phenomena or spin–rotational interactions in the high-temperature region.

The substitution of Sb atoms by Bi ones in MACA seems not to affect the values of the activation energy. The E_a in MACAB is comparable to that found in MACA [13] (6.5 and 5.0 kJ mol^{-1}, above and below T_c, respectively). On the other hand an increase was observed in the value of T_1 for mixed crystals in comparison to that measured in MACA in the high- as well as in the low-temperature phases.

3.6. Dielectric studies

Dielectric properties of MACA and MACB as a function of temperature are known for frequencies lower than 10 kHz. For this reason we extended our studies up to the microwave frequency region for the mixed crystals. The single crystals of MACA break up at T_c so

the dielectric results in the low-temperature phase (II) for that crystal were only qualitative [7]. The mixed crystals, MACAB (for $x > 8\%$), do not break up when passing through the transition.

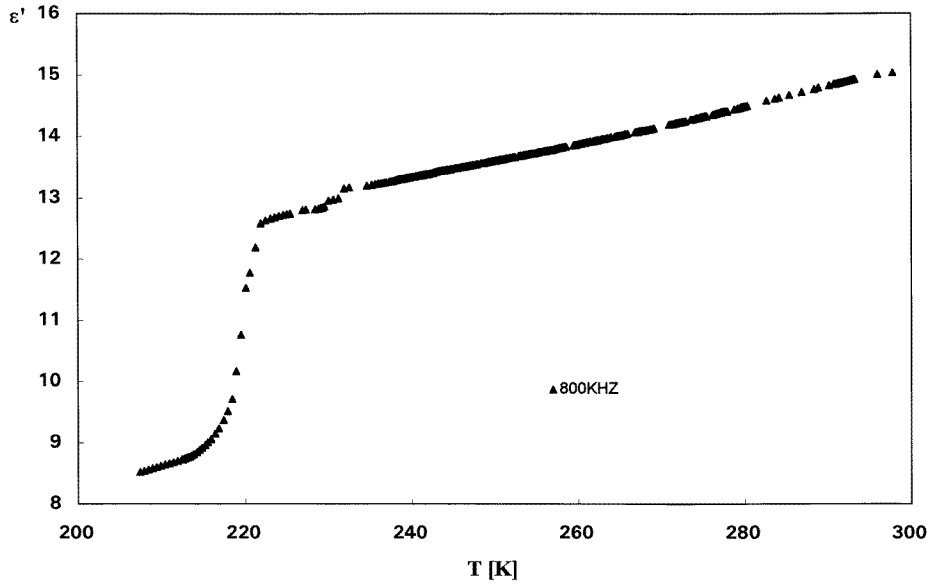

Figure 7. The temperature dependence of the electric permittivity measured along the a axis on cooling, at 800 kHz and 900 MHz for $(CH_3NH_3)_3Sb_{2(1-x)}Bi_{2x}Cl_9$ ($x = 0.22$).

Figures 7 and 8 show the temperature dependence of the real part of electric permittivity (ε') along the a axis at 800 kHz and 900 MHz and along the c axis at 800 kHz, respectively, for the mixed crystals ($x = 0.22$) on cooling. Measurements of the complex electric permittivity for the a axis in the frequency range 1–900 MHz did not reveal any relaxational process. Within the experimental error the value of ε_a is the same over the high-temperature phase. In contrast to the case of the MACA crystal (see figure 3 in [7]) where $\varepsilon_a(T)$ and $\varepsilon_c(T)$ were found to be the same in the high-temperature phase, in the $x = 0.22$ compound a marked 'softening' of ε_a is observed on approaching T_c. A comparison of the dielectric properties along the b axis for the pure analogues (A, antimony, C, bismuth) and the mixed crystal ($x = 0.22$) is presented in figure 9. It is clearly seen that an increase of Bi concentration diminishes the value of ε_b and changes the nature of the phase transition. At the phase transition ($T_c = 220$ K, on cooling) ε drops by two to four units along all directions and after that still decreases for $x = 0.22$. We note that close to room temperature the ε' value for all directions is relatively large but along the b axis the electric permittivity is distinctly raised both above and below T_c. The dielectric anomaly at 247 K in MACB corresponding to the structural phase transition found by NQR [3] and DSC [8] is only indicated by a change in the slope. This anomaly was not detected by earlier dielectric measurements [8, 9] in the low-frequency region.

The dependence of the temperature of phase transition on substitution of Sb by Bi atoms was systematically studied. The mole weight per cent composition and temperature of the phase transition are listed in table 6. As the concentration of bismuth atoms increases the phase transition temperature is gradually shifted towards higher temperatures. Above

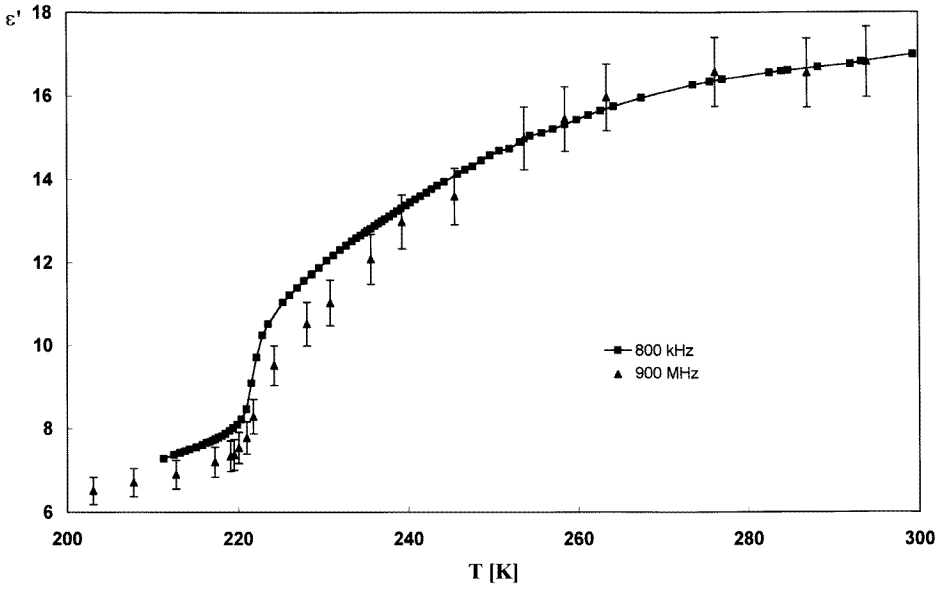

Figure 8. The temperature dependence of the electric permittivity measured along the *c* axis on cooling, at 800 kHz for $(CH_3NH_3)_3Sb_{2(1-x)}Bi_{2x}Cl_9$ ($x = 0.22$).

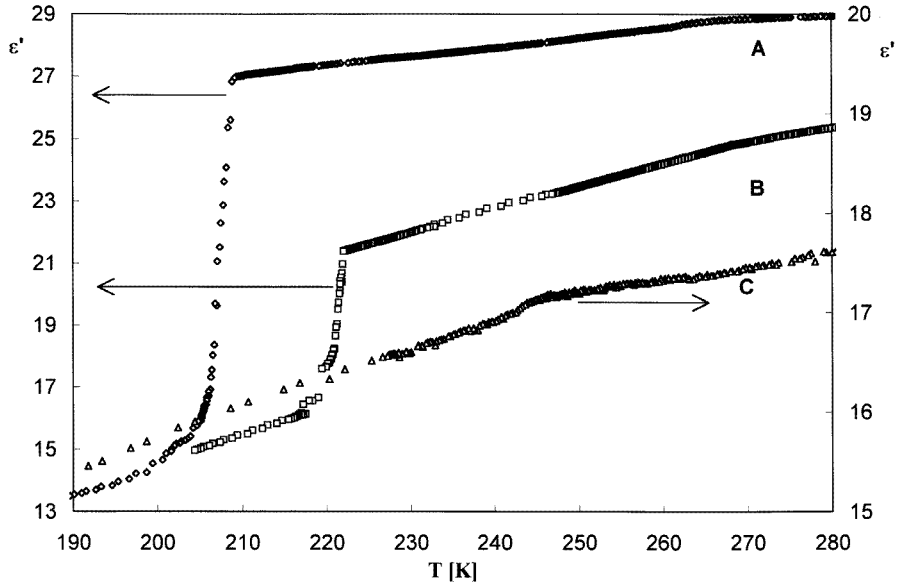

Figure 9. The temperature dependence of the electric permittivity along the *b* axis, on cooling, at 1 MHz for $(CH_3NH_3)_3Sb_2Cl_9$ (A), $(CH_3NH_3)_3Sb_{2(1-x)}Bi_{2x}Cl_9$ ($x = 0.22$) (B) and $(CH_3NH_3)_3Bi_2Cl_9$ (C) (taken from [10]).

the 22% bismuth concentration the T_c value seems to be weakly dependent on the Bi concentration.

Table 6. The dependence of the phase transition temperature on the bismuth concentration.

	$x = 0\%$	$x = 8\%$	$x = 22\%$	$x = 32\%$	$x = 34.5\%$
T_c (K)	208.5	211.0	220.0	220.0	222.5

Dielectric studies for the mixed systems showed that the substitution of antimony by bismuth influences both the dynamics of methylammonium cations and the change of polarizability of the $(Sb_{2(1-x)}Bi_{2x}Cl_9^{3-})_n$ polyanionic form which contributes to the electric permittivity. The observed dielectric anisotropy indicates that permanent dipole moments connected with one of the two non-equivalent methylammonium cations performing isotropic rotation may contribute to the electric polarizability along all the crystallographic directions.

The change in the dielectric function of $\varepsilon'(T)$ in the vicinity of T_c for mixed crystals with low bismuth concentration up to 22% is characteristic of the crystals exhibiting a rotational phase transition with plastic-like high-temperature phases, as in the case of MACA. For MACA and mixed crystals the dipole–dipole interactions are rather weak in the vicinity of the phase transition point, whereas in the case of mixed crystals with increasing bismuth concentration these interactions seem to weaken. This may be consistent with the second-moment NMR studies on the mixed compound. These studies showed that the rotation of $CH_3NH_3^+$ cations is easier in mixed crystals than in pure antimony analogue. The electric permittivity along the *b* and *c* crystallographic directions up to 1 MHz and for the *a* axis up to 1 GHz may be taken as a static permittivity.

The lack of the dielectric dispersion in the microwave region for the mixed crystals and probably the pure antimony analogue (up to 1 GHz) points to a very fast reorientational motion of the electric dipoles connected with the $CH_3NH_3^+$ cations (macroscopic relaxation times shorter than 10^{-11} s).

Comparing our dielectric results with those obtained for other methylammonium halogenoantimonates or bismuthates (III) showing a weak dipole–dipole interaction one can state that the rapid reorientational motion of the dipole groups is a characteristic feature of such systems.

4. Conclusions

From the analysis of properties of mixed crystals presented in this paper we conclude the following.

The substitution of Sb by Bi atom in $(CH_3NH_3)_3Sb_2Cl_9$ crystals drastically affects the nature of the low-temperature structural phase transition ($T_c = 208.5$ K; $x = 0$). A clear first-order transition is observed for MACA ($x = 0$), whereas nearly continuous transformation appears for the crystals with the Bi concentration higher than 30%. The same, close to second-order, transition was detected in MACB ($x = 1$) at 247 K by DSC measurements [8].

The methylammonium cations which are disordered above T_c, N(2)–C(2) and N(3)–C(3), contribute to both the mechanism of the phase transition and the value of the electric permittivity. This is reflected as a distinct decrease in the jump of $\Delta\varepsilon$ at T_c and a diminishing of the value of ε over the high-temperature phase.

Dielectric dispersion studies in mixed crystals revealed a rapid reorientational motion of $CH_3NH_3^+$ cations with the macroscopic relaxation time, τ, shorter than 10^{-11} s.

The NMR studies suggest that the rotational motion of non-equivalent methylammonium cations becomes easier in the phase transition region with increasing bismuth concentration with respect to the situation observed in the pure antimony analogue. This is the reason for the weaker dipole–dipole interactions of methylammonium cations.

Acknowledgments

The authors are grateful to Professor Z Galdecki (Technical University of Lódź, Poland) for allowing the use of the Siemens SHELXTL PC program system in his laboratory.

This work was supported in part by the Committee for Scientific Research within project 3P 40705605.

References

[1] Jakubas R and Sobczyk L 1990 *Phase Transitions* **20** 163
[2] Varna V, Bhattarcharjee R, Vasan H N and Rao C N R 1992 *Spectrochim. Acta* A **48** 1631
[3] Ishihara H, Watanabe K, Iwata A, Yamada K, Kinoshita Y, Okuda T, Krishnan V G, Dou S and Weiss A 1992 *Z. Naturf.* a **47** 65
[4] Mackowiak M, Weiden N and Weiss A 1990 *Phys. Status Solidi* a **119** 77
[5] Kozioł P, Furukawa Y and Nakamura D 1991 *J. Phys. Soc. Japan* **60** 3850
[6] Kozioł P, Furukawa Y, Nakamura D and Jakubas R 1992 *Bull. Chem. Soc. Japan* **65** 1707
[7] Jakubas R, Czapla Z, Galewski Z, Sobczyk L, Żogał O J and Lis T 1986 *Phys. Status Solidi* a **93** 449
[8] Belkyal I, Mokhlisse R, Tanouti B, Chanh N B and Couzi M 1992 *J. Alloys Compounds* **188** 186
[9] Jakubas R, Tomaszewski P and Sobczyk L 1989 *Phys. Status Solidi* a **111** K27
[10] Jakubas R, Decressain R, Bator G and Lefebvre J *Physica* B submitted
[11] Belkyal I, Mokhlisse R, Tanouti B, Chanh N B and Couzi M 1993 *Phys. Status Solidi* a **136** 45
[12] Bator G, Jakubas R and Malarski Z 1991 *J. Mol. Struct.* **246** 193
[13] Decressain R, Jakubas R and Lefebvre J 1995 *Phys. Status Solidi* a **147** K73
[14] Kucharczyk D, Pietraszko A and Łukaszewicz K 1993 *J. Appl. Crystallogr.* **26** 467
[15] SHELXTL PC Program System, Siemens Analytical X-ray Instruments Inc., Madison, WI 1990
[16] Kihara K and Sudo T 1974 *Acta Crystallogr.* B **30** 1088
[17] Furukawa Y and Nakamura D 1989 *Z. Naturf.* a **44** 1122
[18] Ishida H, Ikeda R and Nakamura D 1986 *Bull. Chem. Soc. Japan* **59** 915
[19] Ishida H, Takagi K, Iwachido T, Terashima M, Nakamura D and Ikeda R 1990 *Z. Naturf.* a **45** 923